Ultrasound for Periodontal Imaging

5

Lawrence H. Le, Kim-Cuong T. Nguyen, Neelambar R. Kaipatur, and Paul W. Major

5.1 Periodontium

The periodontal complex has four main entities: the gingiva, cementum, periodontal ligament, and alveolar bone (Fig. 5.1). Although the uniqueness of each structure helps distinguish them from each other, the periodontium as one entity helps provide the necessary support for the teeth in which they are embedded. The gingiva forms the collar around the tooth and the alveolar bone covering, and is divided into unattached, marginal, or free gingiva, and attached gingiva [1]. The keratin in the attached gingiva gives its strength and toughness to adhere to the tooth and alveolar bone [2]. The attached gingiva functions to protect the tissue from receding and to protect the periodontal ligament from bacterial invasion [3]. The cementum is the outermost layer of the tooth root covering the root dentin and serves to anchor the periodontal ligament fibers. It is broadly classified into acellular and cellular cementum [4]. The periodontal ligament is a thin layer of connective tissue that surrounds the tooth, and attaches the cementum of the tooth root to the alveolar bone. The periodontal fibers are strong and oriented in different directions

L. H. Le (✉)
Department of Radiology and Diagnostic Imaging, University of Alberta, Edmonton, AB, Canada
School of Dentistry, University of Alberta, Edmonton, AB, Canada
Department of Biomedical Engineering, University of Alberta, Edmonton, AB, Canada
e-mail: lawrence.le@ualberta.ca

K.-C. T. Nguyen
Department of Radiology and Diagnostic Imaging, University of Alberta, Edmonton, AB, Canada
Department of Biomedical Engineering, University of Alberta, Edmonton, AB, Canada
e-mail: cuong1@ualberta.ca

N. R. Kaipatur · P. W. Major
School of Dentistry, University of Alberta, Edmonton, AB, Canada
e-mail: kaipatur@ualberta.ca; major@ualberta.ca

H.-L. (Albert) Chan, O. D. Kripfgans (eds.), *Dental Ultrasound in Periodontology and Implantology*, https://doi.org/10.1007/978-3-030-51288-0_5

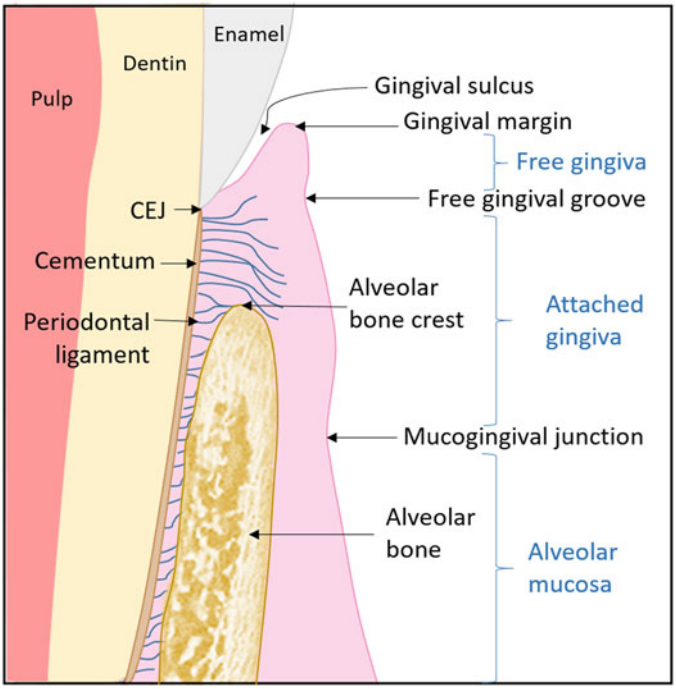

Fig. 5.1 The periodontium

to withstand loading forces during chewing [5]. Alveolar bone development and preservation are dependent on the presence of teeth and are subject to remodeling. It comprises the alveolar process of the jaws that houses the developing tooth buds during growth and later becomes the alveolar bone proper that forms the tooth socket and supports the tooth. The alveolar process provides attachment for periodontal ligament and the associated tooth root [6]. Alveolar bone loss can be due to numerous reasons. Dental caries is a common cause for alveolar bone loss as a result of bacterial infection extending to the root apex leading to a periapical abscess and apical bone loss [7, 8]. Other local causes include periodontitis and residual ridge resorption due to tooth loss [9, 10]. Systemic causes of alveolar bone loss include Chediak-Higashi syndrome (CHS), osteoporosis, Down syndrome, Papillon-Lefevre syndrome (PLS), HIV infection, and neutropenia [11, 12].

5.2 Current Clinical Methods to Assess Periodontium

Periodontitis or periodontal (gum) disease (Fig. 5.2) is one of the most common oral health problems. Prevalence increases with age and it affects a significant percentage of the world population [13]. 15% of the middle-aged adults and twice as many seniors suffer from periodontal disease [14]. The most common signs

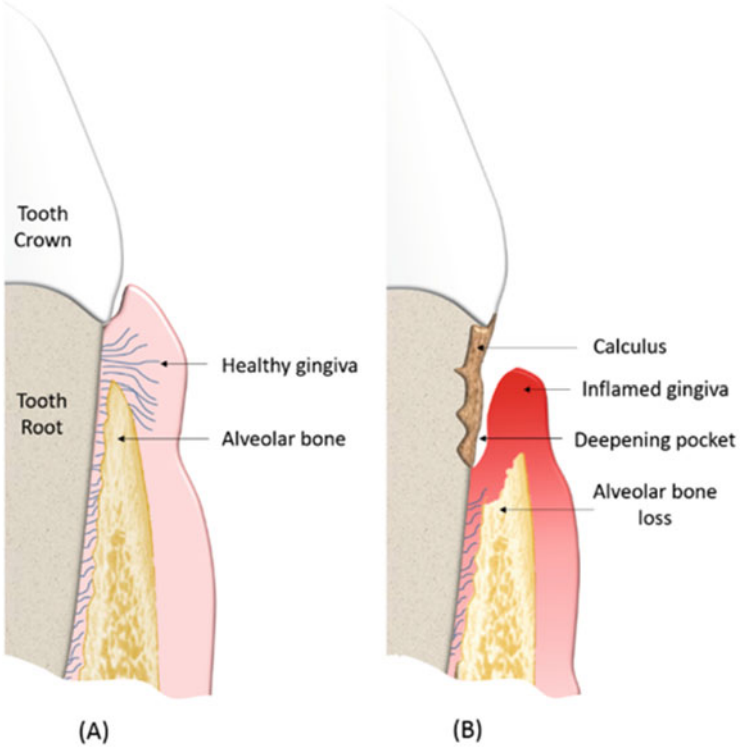

Fig. 5.2 Periodontal disease: (**a**) healthy and (**b**) diseased

include inflammation, bleeding on probing, increased pocket depth, and clinical attachment loss, culminating in alveolar bone loss and eventual tooth loss [1]. Periodontal probing is one of the most common diagnostic tools used by dentists to measure pocket depth and clinical attachment level [15]. Two inherent drawbacks associated with periodontal probing include the invasiveness of the procedure and lack of measurement accuracy in individuals with extensive gingival inflammation and low pain threshold. In addition, periodontal probing does not accurately measure alveolar bone level, which is an important measure of disease state [16].

Consistent and accurate measurement requires a reliable identification landmark. The cementoenamel junction (CEJ) or cervical line is defined as a line on the surface of a tooth where the enamel on the crown meets the cementum on the root. The CEJ is considered a stable landmark and is used as a reference marker to evaluate alveolar bone level and accurately measure gingival recession and clinical attachment loss [17]. A periodontal probe (Fig. 5.3) reliably measures the distance from the CEJ to the bottom of the gingival sulcus [18], but the drawbacks include challenges with tactile visualization of the CEJ and invasiveness of the procedure as described above.

Due to the inherent difficulties with alveolar crest identification using the traditional clinical probing method, radiography was until recently considered

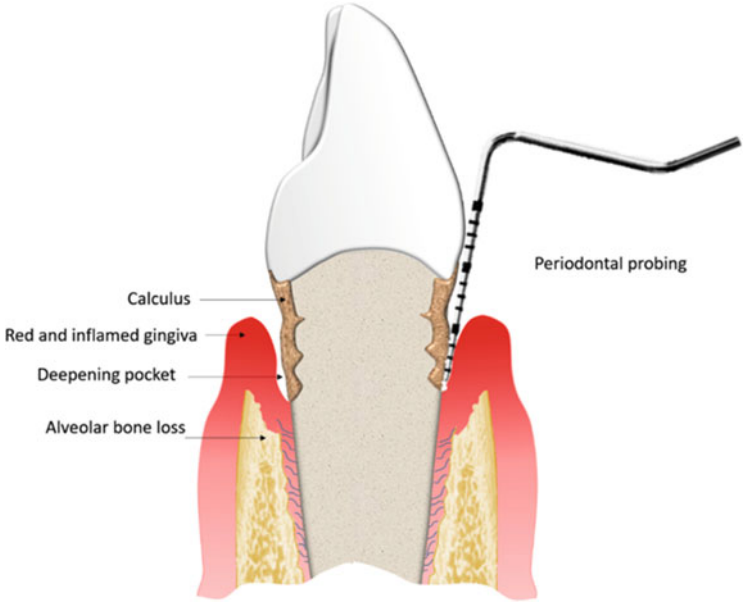

Fig. 5.3 Periodontal probing

the gold standard and a non-invasive method to detect CEJ and alveolar bone crest. Panoramic radiograph (Fig. 5.4a) is useful as an overall screening image to identify the dentoalveolar structures but does not provide the accuracy or sufficient resolution for periodontal diagnosis and treatment planning. Intraoral radiographs (Fig. 5.4b) have the resolution and structural detail to locate alveolar crest on the mesial and distal aspects of tooth roots, but the overlapping tooth structures render it hard to visualize on the buccal and lingual surfaces of the teeth in the two-dimensional (2D) periapical image [19].

Innovative methods using computer-assisted localization (CAL) of CEJ in digital radiographs were introduced in 1989 [20]. Although digital radiographs led to faster acquisition and instant identification, the inherent drawback of inability to locate the buccal and palatal CEJ lines in periapical films was still evident. Cone-beam computerized tomography (CBCT) has been shown to make available, fast, and accurate 3D volumetric image reconstruction and visualization of internal anatomical features that 2D intraoral and panoramic images have had difficulty to display [21–23] (Fig. 5.5). CBCT images have been used to measure the distance from a reference landmark such as CEJ to alveolar bone crest. Accuracy of the CBCT measurements has been demonstrated in a number of peer-reviewed articles. In an in vitro study on dry human skulls, Leung et al. [24] reported a measurement error of 0.4 mm for CEJ and 0.6 mm for alveolar bone crest identification from a known reference point as compared to direct measurement as the gold standard. The accuracy of CBCT with respect to intraoral radiography was also established

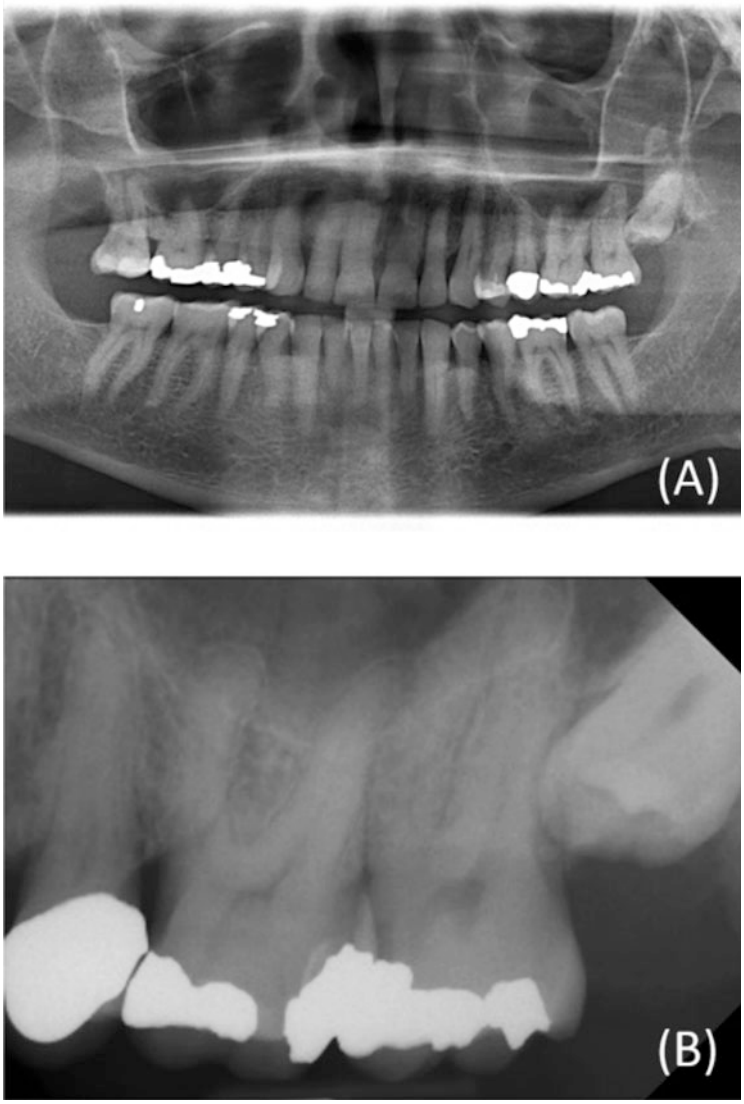

Fig. 5.4 Examples of 2D radiographs: (**a**) panoramic and (**b**) periapical

for identification of vertical bony defects in an in vivo study involving human subjects [25]. The biggest advantage of a CBCT image is the 3D visualization of the structures on the buccal (cheek), labial (lip), and lingual (tongue) sides, without any overlap from other hard tissues such as teeth [26]. Unfortunately, CBCT has increased radiation dose, which is 5–74 times higher than a single panoramic radiograph. The added dose accumulation with repeated imaging that is necessary to track progression of periodontal disease is unwarranted [27]. Although recent

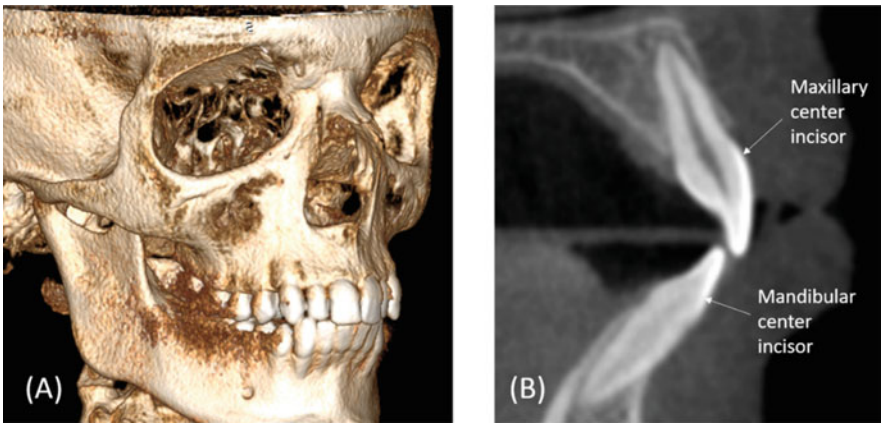

Fig. 5.5 CBCT imaging: (**a**) 3D reconstruction of a human skull and (**b**) cross-section of upper and lower incisor teeth

systematic reviews [21, 26] concluded that CBCT is the standard of care to identify intra-bony periodontal defects and furcation defects, the authors also emphasized that the financial burden of procuring a dental CBCT unit and the excessive radiation dose preclude the routine use of CBCT. The radiation risk is much higher in pediatric population due to its impact on growth potential and early development of cancer [28]. Low and medium resolution CBCT does not have sufficient spatial resolution to accurately identify the CEJ and alveolar crest [29]. Figure 5.6 displays CBCT and μCT images of a porcine incisor for comparison. The image was scanned by an i-CAT 17-19 dental CBCT unit (Imaging Sciences International, Hatfield, PA, USA) with a voxel size of 200-µm and a 16 cm $\times$ 56 cm field-of-view (FOV). As seen from Fig. 5.6a, the edges of the hard tissues are not well defined, and it is difficult to identify the CEJ and alveolar bone accurately. Achieving better resolution using small FOV imaging and smaller voxel size can result in higher radiation dose [30].

For comparison, the μCT image (Fig. 5.6b), which was scanned by a MILABS U-SPECT4 CT system (Utrecht, The Netherlands) with an 18-µm voxel, shows a distinct enamel layer that is in contrast to underlying dentin and the cementum with a clearly identifiable alveolar bone crest. This leads us to believe that the μCT can be considered a gold standard for accuracy in identifying key periodontal landmarks, but the miniaturization of the equipment limits its application for in vitro studies or small animal research.

5.3 Ultrasound Imaging

Ultrasound is a mechanical wave with frequency higher than 20 kHz. It is generated and detected by a transducer, comprised of one or more crystal elements of dipole-like piezoelectric material. The elements convert electrical energy into mechanical deformation of the crystals and conversely generate electrical signals by the defor-

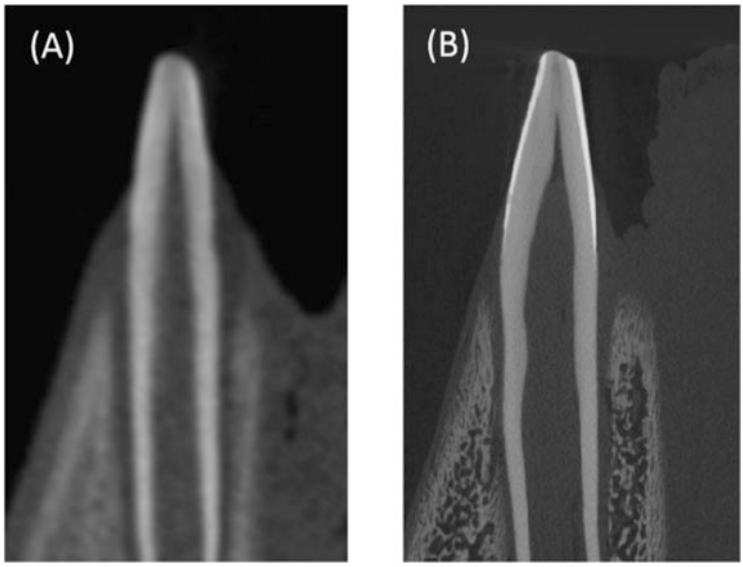

Fig. 5.6 Imaging of a porcine incisor: (**a**) a CBCT image and (**b**) a μCT image

mation of the elements due to external pressure. The passing of ultrasound through the tissue shakes the tissue particles around their neighborhood. The vibrating particles initiate the motion of their neighboring particles, thus transmitting the ultrasound energy from one place to another without the migration of the particles. However, the particles must expend energy to overcome the frictional forces among particles to pass the energy, and the amount of energy loss is characterized by the attenuation coefficient of the tissue. In the context of ultrasound imaging, the tissue is characterized by the density, speed of ultrasound, and attenuation coefficient, where the product of density and velocity is known as acoustic impedance. The generation and propagation of ultrasound within the tissue is strictly mechanical without involvement of ionizing radiation.

Ultrasonography is an imaging technique to use the reflections or echoes of the ultrasound signals to image the internal structures of the tissues. The strength of the returning echoes is governed by the acoustic impedance contrast of the interface separating the media. Energy partition will take place at the interface, i.e., part of the energy will be reflected, while the rest will be transmitted across the interface, which is an ideal situation when scattering and attenuation of ultrasound energy are ignored. Ultrasound is a non-invasive, ionizing-radiation free, economical, and painless diagnostic tool for hard and soft material imaging, and is used in many fields, especially in medicine and engineering. Medical ultrasound has been routinely used to image soft tissues with frequencies ranging from 2 to 15 MHz. Ultrasound has also been applied to characterize bone tissue [31], to estimate the cortical thickness [32], and to image scoliotic spine in children [33]. The bone/soft

tissue interface strongly reflects ultrasound energy, thus making bone tissue imaging possible.

The use of ultrasound in dentistry, primarily in periodontics, has been the subject of research for many years but has not been adopted for routine imaging. Ultrasound has been considered a promising tool for imaging hard dental structures. In early 1960s, Baum et al. [34] claimed to identify enamel-dentin and dentin-pulp interfaces using freshly extracted teeth and 15-MHz pulse-echo ultrasound. Subsequent research effort has mainly been focused on ex vivo studies of hard tissues using radio-frequency data instead of images [35]. Although imaging studies of the dento-periodontium are limited, recent literature suggests the potential use of ultrasound imaging in periodontal diagnosis as a good alternative to radiographic imaging due to the increased radiation dose associated with the latter and potential harmful effect on an individual's health. Interpretation of ultrasound images requires specific expertise and is a major challenge for dental clinicians. This may represent a significant barrier for adoption as a routine diagnostic tool in the field of dentistry.

5.3.1 Ex Vivo Imaging

Tsiolis et al. [36] used a 20-MHz ultrasonic scanner, designed for dermatological use, to image the porcine periodontium. The scanner was equipped with a single transducer translated by a motor to produce a 15-mm B-mode image of the internal periodontal structures. By comparing linear measurements between a manually created notch in the enamel and the alveolar crest, they found the ultrasound measurements had better repeatability than the direct measurement and transgingival probing. Chifor et al. [37] also used a similar ultrasonic scanner to study pig mandibles and found accurate measurements of periodontal space width, alveolar bone thickness, and gingiva thickness. Their results also demonstrated a much higher positive correlation between ultrasound and CBCT ($R = 0.98$, $p < 0.01$) than that between ultrasound and microscopy ($R = 0.79$, $p < 0.0001$). Nguyen et al. [38] used a single 20-MHz transducer to image six porcine lower central incisors and found unambiguous identification of the CEJ, enamel, dentin, and cementum. They also found μCT and ultrasound measurements were in strong agreement. Nguyen et al. [39] also imaged hard dental tissues and periodontal attachment apparatus using a 20-MHz portable medical diagnostic SonixTablet ultrasound phase array system (Analogic, Vancouver, BC, Canada). The system had an 8–40 MHz array transducer comprised of 128 elements of 0.1-mm pitch with a small 4 mm $\times$ 13 mm array footprint. The scanner was capable to operate up to 40 MHz with hardware upgrade. The lateral and axial resolutions of the ultrasound probe were 0.50 mm and 0.20 mm, respectively. Further, they analyzed the echoes coming from the interfaces and interpreted their existence in terms of traveling time and signal simulation.

Figure 5.7a shows the center incisors of a mandible from a 4-month-old piglet [39]. The experimental setup is shown in Fig. 5.7b, where the transducer straddled the tooth and gingiva on the labial side. A piece of 4-mm gel pad was placed between

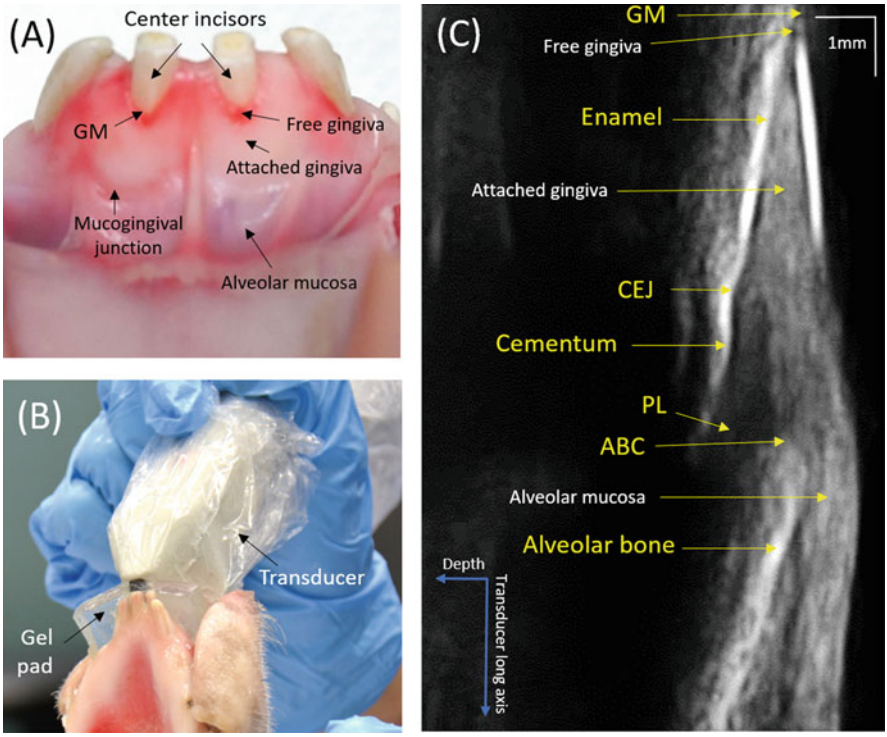

Fig. 5.7 Ultrasound scan of a porcine incisor: (**a**) the mandible, (**b**) the transducer aligned with the long axis of a center incisor, and (**c**) the corresponding ultrasound image of the center incisor

the transducer and the tooth tissue to ensure good coupling between the contact areas. Another purpose of the gel pad was to keep the region of interest within the focal zone of the ultrasound beam. The presence of the gel pad also created echoes from the gel pad-enamel and gel pad-gingiva interfaces, which makes measurement of the gingival thickness possible. The scanning started with the transducer over the enamel and ended with the transducer over the gingiva by sliding the transducer slowly along the long axis of the tooth.

A frame of a video clip, showing the cross-section of a B-mode ultrasound image, is shown in Fig. 5.7c. The interfaces of the enamel and cementum are sharp and well defined as they are strong reflectors and have high acoustic impedance contrast with gingiva [39]. The alveolar bone layer is porous and the pores scatter ultrasound energy. Therefore, the image of the bone layer is blurred but visible and the alveolar crest is clearly identified. The section of gingiva close to the gingival margin has strong reflection as compared to the rest of the gingiva. This happens in most cases for porcine samples because this part of gingiva is denser. In contrast to the CBCT image, the CEJ can be visually recognized. The enamel has much higher speed of ultrasound and density than the gingiva. As the enamel becomes thinner when it approaches the CEJ, more low-speed gingiva fills in the place. Ultrasound takes

longer to reach the CEJ area and therefore the image shows a concave region with "the peak of the hump" toward left. The image does not show a continuation of the cementum beyond the alveolar crest. This is because ultrasound cannot penetrate through thick alveolar process. Thickness of the gingiva can be measured from the ultrasonograph, which is impossible in the CBCT image. Nguyen et al. [39] further compared the measurements from ultrasound and CBCT images and found the difference between these measurements were within 10%, showing ultrasound is as good as CBCT in providing clinically relevant information. The gel pad-enamel and gingiva-enamel interfaces have large acoustic impedance contrast, resulting in strong reflection. Therefore, strong hyper-echoic signals are expected, as evidenced by the enamel reflector.

5.3.2 In Vivo Imaging

Fukukita et al. [40] appear to be the first group to produce early in vivo B-scan images of the tooth and alveolar bone using a single 20-MHz transducer with a mechanical driving motor. Salmon and Le Denmat [41] developed a 25-MHz single transducer ultrasound prototype system to perform ultrasound imaging on healthy volunteers. The transducer was linearly translated to provide continuous scanning for a B-mode image, which showed the cementum and the alveolar process. Zimbran et al. [42] imaged periodontal structures of human premolars in vivo using a very high frequency (40 MHz) Ultrasonix SonoTouch scanner. While the scanning set up was not provided, it was expected that the transducer was placed extra-orally on the cheek to image the premolars. In a recent study, Chan et al. [43] studied 144 teeth from 6 fresh cadavers by means of 14-MHz ultrasound, CBCT with 80 μm resolution, and direct measurement. By comparing the alveolar bone level with respect to CEJ and the thickness of the bone crest, they found the ultrasound measurements were as accurate as CBCT and direct measurements.

The scanning setup for human incisors is shown in Fig. 5.8a. The subject was a 15-year-old male volunteer. The long axis of the transducer lined up with the long axis of the tooth. The transducer had a clip at its front to hold a small piece of gel pad. Figure 5.8b shows an ultrasound B-mode image. The image shows clearly enamel boundary, CEJ, gingival margin (GM), gingiva, cementum, alveolar bone crest (ABC), alveolar bone, and periodontal ligament (PL). The portion of cementum underlying the alveolar bone cannot be seen as expected because ultrasound cannot penetrate through thick bone.

5.4 Discussion

CBCT is a valuable clinical imaging tool for assessing alveolar bone and providing evidence-based treatment. It allows reconstruction of any sectional views without overlying tissue obstruction, thus allowing a clear visualization of the alveolar structures on the lingual and buccal sides. However, the identification of CEJ on

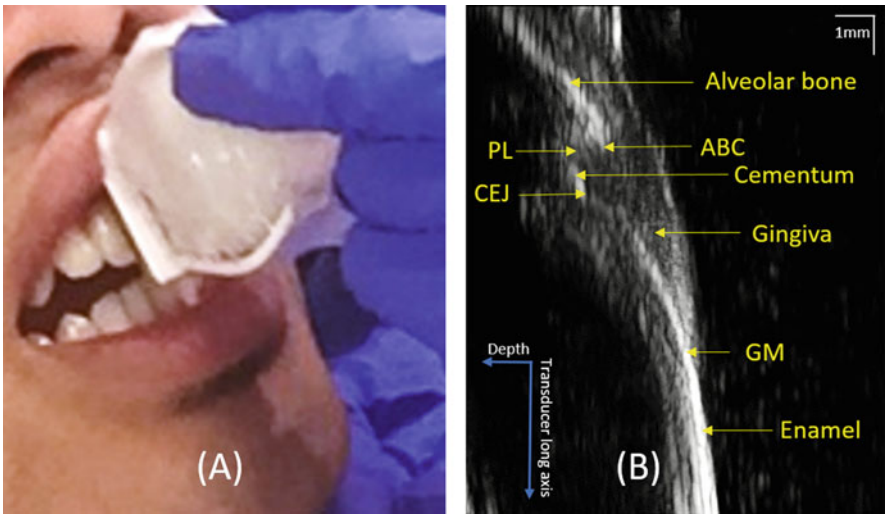

Fig. 5.8 Ultrasound scan of a human incisor: (**a**) scanning configuration and (**b**) ultrasound image

CBCT images is still a challenge [39] unless high-resolution CBCT is employed, which will require much higher radiation exposure to patients. Furthermore, dental CBCT is not suitable for soft tissue imaging such as gingival characterization and measurement. Development of diagnostic high-quality imaging modality without ionizing radiation is highly desirable. Reports on recent research have demonstrated that high frequency ultrasound is ionizing radiation-free and has the potential to visualize alveolar bone on the buccal and lingual surfaces, diagnose periapical inflammatory lesions [44, 45], and measure sulcus depth and gingival thickness [42]. The use of multi-element array transducer has significantly reduced the data acquisition time to few seconds, thereby decreasing patient chair time and minimizing the impact of patient motion to degrade the image quality. A phase array ultrasound equipped with multi-element transducer is preferable to a single transducer translated by a motor to generate a B-mode image. The former system will steer all elements electronically to focus on a depth point to generate one A-line, which greatly enhances the signal-to-nose ratio. The image, which is made up of many A-lines, can be obtained by sweeping the beam across the target. The quality of the image is much superior to that of a single element transducer with translation. However, one current drawback is the size of the transducer, which presently restricts intraoral use to incisors or canines. Small, compact, and flexible transducers need to be designed to study premolars and molars intraorally.

Periodontal tissues are complex with tissues of different scales such as gingiva, alveolar bone, cementum, and periodontal ligament. Imaging these hard and soft tissues require different ultrasound frequency or wavelength as their speeds span from 1540 m/s (gingiva) to 3200 m/s (cementum). In principle, using high frequency will increase imaging resolution to see small details or scales. However, the intrinsic

attenuation characteristics of oral tissues have preferential filtering to remove high frequencies faster than low frequencies as the signal travels through the tissues. As high frequency components are removed, the wavelength of the probing signal becomes larger and the signal becomes less sharp, thus losing the originally required resolution to look at small scales. Acoustic attenuation usually increases with frequency [46] and places a limitation to depth penetration of the ultrasound signal. Thus, a compromise must be made to choose a center frequency to balance between imaging depth and imaging details.

Alveolar bone is cancellous bone covered by a thin cortical bone. Assuming that the acoustic impedances of gingiva and cortical bone are 1.63 MRayl [39] and 7.38 MRayl [47], respectively, the echoes carry approximately 41% of the incident energy but delineate a good estimation of the gingiva-alveolar bone interface. The bone surface is neither regular nor smooth. The rough surfaces of the pores tend to scatter ultrasound in all directions. The scattering process has two negative impacts. First, the scattered energy will not be received by the transducer, thus creating an apparent loss of the signal's energy; second, the scattered signals are considered noise, generating speckle characteristics in the image, which reduces image contrast and thus the diagnostic quality of the image. Due to scattering, the gingiva-alveolar bone interface is blurred and fuzzy. This is also a reason why most of the ultrasound images published so far lack good diagnostic quality and clarity. Even though in theory, there is about 59% incident energy transmitted across the gingiva-alveolar bone interface into the alveolar bone, the actual amount of incident energy striking the bottom of the alveolar layer is less due to scattering and attenuation within the alveolar bone composition. Therefore, the corresponding echoes are less likely to be detected. For this reason, the thickness of the alveolar bone could not be determined [37, 41]. Löst et al. [48] recognized the cancellous bone as the limiting factor to prevent the identification of the underlying periodontal space in the ultrasound images.

Overall, high frequency ultrasound is desirable as it generates signals of smaller wavelength, which can be used to study small-scale structures. However, high frequency signals cannot propagate greater depth due to intrinsic attenuation of the tissue and being easily scattered by small inhomogeneities, thus affecting the image quality. A study using a range of center frequencies should be investigated to find an optimal frequency for intraoral applications such as identification of soft tissue thickness for non-invasive implant placements including orthodontic mini-implants (temporary anchorage devices), fenestration and dehiscence defects, furcation and bony defects, periapical pathology including identification of cysts and granulomas, submerged and ectopic teeth localization, and sutural width. Ultrasound can potentially be used for evaluating disease progression and treatment effects especially in periodontal regeneration procedures and orthodontics. In contrast to radiography, ultrasound imaging demands more technical skills from the operator in addition to an understanding of ultrasound physics, which can be a barrier entailing slow adoption of the imaging technique in dentistry. Training in image acquisition and image interpretation is important for dental professionals to understand the technique and its capabilities in order to adopt the new technology.

Application of image processing techniques is important to enhance signal-to-noise ratio and contrast of the images. Pattern recognition algorithms and machine learning will also play a pivotal role in aiding clinicians to automatically identify anatomic structures and diagnostic features in ultrasound images [49–52].

Though the feasibility of using ultrasound to study dento-periodontal tissues has been confirmed, the accuracy and validity of ultrasound imaging as a diagnostic tool have not been adequately studied due to small number of published reports and small sample size used for the studies [39, 53]. Further studies using sufficiently large sample sizes of ex vivo and especially in vivo data are warranted to establish satisfactory level of confidence for ultrasound imaging.

5.5 Conclusion

Although ultrasound research is in its infancy, it has shown significant potential as a diagnostic tool in dentistry. Since ultrasound does not expose the patient to ionizing radiation, imaging can be done routinely on children and can be repeated at regular intervals to assess change over time. The potential of ultrasound to be a routine diagnostic tool in every dental office, like an intraoral X-ray unit, is in the near future.

Acknowledgments The authors thank the Women and Children's Health Research Institute (WCHRI), Canada for the financial support of a Seed Grant. The work was partly supported by LH Le's NSERC Discovery Grant. KCT Nguyen acknowledges the support from Alberta Innovates for the PhD fellowship.

References

1. Newman MG, et al. Newman and Carranza's clinical periodontology e-book. Elsevier Health Sciences; 2018. ISBN:032353323X.
2. Cohen L. Keratinization of the gingivae. Dent Pract Dent Rec. 1967;18.4:134–8. ISSN:0011-8729.
3. Ainamo J, Löe H. Anatomical characteristics of gingiva. A clinical and microscopic study of the free and attached gingiva. J Periodontol. 1966;37.1:5–13. ISSN:1943-3670.
4. Foster BL. On the discovery of cementum. J Periodontal Res. 2017;52.4:666–85. ISSN:0022-3484.
5. De Jong T, et al. The intricate anatomy of the periodontal ligament and its development: lessons for periodontal regeneration. J Periodontal Res. 2017;52.6:965–74. ISSN:0022-3484.
6. Goldman HM. Alveolar bone in health and disease, possibilities of reattachment. J Dent Med. 1948;3.2:30. ISSN:0096-0241.
7. Stashenko P, Yu SM, Wang C-Y. Kinetics of immune cell and bone resorptive responses to endodontic infections. J Endod. 1992;18.9:422–6. ISSN:0099-2399.
8. Chu T-MG, Liu SS-Y, Babler WJ. Craniofacial biology, orthodontics, and implants. In: Basic and applied bone biology. Amsterdam: Elsevier; 2014. p. 225–42.
9. Manson JD. Bone morphology and bone loss in periodontal disease. J Clin Periodontol. 1976;3.1:14–22. ISSN:0303-6979.
10. Beube FE. Correlation of degree of alveolar bone loss with other factors for determining the removal or retention of teeth. Dent Clin North Am. 1969;13.4:801. ISSN:0011-8532.

11. Kinane DF, Marshall GJ. Periodontal manifestations of systemic disease. Aust Dent J. 2001;46.1:2–12. ISSN:0045-0421.
12. Jeffcoat MK. Bone loss in the oral cavity. J Bone Miner Res. 1993;8.S2:S467–73. ISSN:0884-0431.
13. Pihlstrom BL, Michalowicz BS, Johnson NW. Periodontal diseases. Lancet. 2005;366.9499:1809–20. ISSN:0140-6736.
14. Web Page. 2014. http://www.cda-adc.ca/_files/about/news_events/health_month/PDFs/dentist_questions_answers.pdf.
15. Listgarten MA. Periodontal probing: what does it mean? J Clin Periodontol. 1980;7.3:165–76. ISSN:0303-6979.
16. Xiang X, et al. An update on novel non-invasive approaches for periodontal diagnosis. J Periodontol. 2010;81.2:186–98. ISSN:0022-3492.
17. Preshaw PM, et al. Measurement of clinical attachment levels using a constant-force periodontal probe modified to detect the cementoenamel junction. J Clin Periodontol. 1999;26.7:434–40. ISSN:0303-6979.
18. Hug HU, et al. Validity of clinical assessments related to the cementoenamel junction. J Dent Res. 1983;62.7:825–9. ISSN:0022-0345.
19. Misch KA, Erica SY, Sarment DP. Accuracy of cone beam computed tomography for periodontal defect measurements. J Periodontol. 2006;77.7:1261–6. ISSN:1943-3670.
20. Haralick RM, Ramesh V, Hausmann E, Allen K. Computerized detection of cemento-enamel junctions in digitized dental radiographs. In: Images of the Twenty-First Century. Proceedings of the Annual International Engineering in Medicine and Biology Society, 1989 Nov 9: p. 1652–54. IEEE.
21. Walter C, et al. Cone beam computed tomography (CBCT) for diagnosis and treatment planning in periodontology: a systematic review. Quintessence Int. 2016;47.1:25–37.
22. K de Faria Vasconcelos, et al. Detection of periodontal bone loss using cone beam CT and intraoral radiography. Dentomaxillofac Radiol. 2012;41.1:64–9. ISSN:0250-832X.
23. Sun L, et al. Accuracy of cone-beam computed tomography in detecting alveolar bone dehiscences and fenestrations. Am J Orthod Dentofacial Orthop. 2015;147.3:313–23. ISSN:0889-5406.
24. Leung CC, et al. Accuracy and reliability of cone-beam computed tomography for measuring alveolar bone height and detecting bony dehiscences and fenestrations. Am J Orthod Dentofacial Orthop. 2010;137.4:S109–19. ISSN:0889-5406.
25. Grimard BA, et al. Comparison of clinical, periapical radiograph, and cone-beam volume tomography measurement techniques for assessing bone level changes following regenerative periodontal therapy. J Periodontol. 2009;80.1:48–55. ISSN:0022-3492.
26. Haas LF, et al. Precision of cone beam CT to assess periodontal bone defects: a systematic review and meta-analysis. Dentomaxillofac Radiol. 2017;47.2:20170084. ISSN:0250-832X.
27. Scarfe WC, Farman AG. What is cone-beam CT and how does it work? Dent Clin North Am. 2008;52.4:707–30. ISSN:0011-8532.
28. Theodorakou C, et al. Estimation of paediatric organ and effective doses from dental cone beam CT using anthropomorphic phantoms. Br J Radiol. 2012;85.1010:153–60. ISSN:0007-1285.
29. Brüllmann D, Schulze RKW. Spatial resolution in CBCT machines for dental/maxillofacial applications—what do we know today? Dentomaxillofac Radiol. 2014;44.1:20140204. ISSN:0250-832X.
30. Li G. Patient radiation dose and protection from cone-beam computed tomography. Imaging Sci Dent. 2013;43.2:63–9. ISSN:2233-7822.
31. Nguyen K-CT, Le LH, Tran TNHT, Sacchi MD, Lou EHM. Excitation of ultrasonic Lamb waves using a phased array system with two array probes: phantom and in-vitro bone studies. Ultrason. 2014;54.5:1178–85.
32. Zheng R, Le LH, Sacchi MD, Lou E. Imaging internal structure of long bones using wave scattering theory. Ultrasound Med Biol. 2015;40.11:2955–65.
33. Chen W, Le LH, Lou E. Reliability of the axial vertebral rotation measurements of adolescent idiopathic scoliosis using the center of lamina method on ultrasound images: in-vitro and in-vivo study. J Euro Spine. 2016;25.10:3265–73.

34. Baum G, et al. Observation of internal structures of teeth by ultrasonography. Science. 1963;139.3554:495–6. ISSN:0036-8075.
35. Barber FE, Lees S, Lobene RR. Ultrasonic pulse-echo measurements in teeth. Arch Oral Biol. 1969;14.7:745, IN3. ISSN:0003-9969.
36. Tsiolis FI, Needleman IG, Griffiths GS. Periodontal ultrasonography. J Clin Periodontol. 2003;30.10:849–54. ISSN:1600-051X.
37. Chifor R, et al. The evaluation of 20 MHz ultrasonography, computed tomography scans as compared to direct microscopy for periodontal system assessment. Med Ultrason. 2011;13.2:120–6.
38. Nguyen K-CT, Le LH, Kaipatur NR, Major PW. Imaging cemento-enamel junction using a 20-MHz ultrasonic transducer. Ultrasound Med Biol. 2016;42.1:333–8.
39. Nguyen K-CT, Le LH, Kaipatur NR, Zheng R, Lou EH, Major PW. High-resolution ultrasonic imaging of dento-periodontal tissues using a multi-element phased array system. Ann Biomed Eng. 2016; 44(10):2874-86. ISSN:0090-6964.
40. Fukukita H, et al. Development and application of an ultrasonic imaging system for dental diagnosis. J Clin Ultrasound. 1985;13.8:597–600. ISSN:1097-0096.
41. Salmon B, Le Denmat D. Intraoral ultrasonography: development of a specific high-frequency probe and clinical pilot study. Clin Oral Investig. 2012;16.2:643–9. ISSN:1432-6981.
42. Zimbran A, Dudea S, Dudea D. Evaluation of periodontal tissues using 40MHz ultrasonography. Preliminary report. Med Ultrason. 2013;15.1:6–9. ISSN:1844-4172.
43. Chan H-L, et al. Non-invasive evaluation of facial crestal bone with ultrasonography. PLoS One. 2017;12.2:e0171237. ISSN:1932-6203.
44. Cotti E, et al. A new technique for the study of periapical bone lesions: ultrasound real time imaging. Int Endod J. 2002;35.2:148–52. ISSN:0143-2885.
45. Musu D, et al. Ultrasonography in the diagnosis of bone lesions of the jaws: a systematic review. Oral Surg Oral Med Oral Pathol Oral Radiol 2016;122.1:e19–29. ISSN:2212-4403.
46. Tole NM, Ostensen H. Basic physics of ultrasonographic imaging. World Health Organization; 2005. ISBN:9241592990.
47. Culjat MO, et al. A review of tissue substitutes for ultrasound imaging. Ultrasound Med Biol. 2010;36.6:861–73. ISSN:0301-5629.
48. Löst C, Irion K-M, Nüssie W. Determination of the facial/oral alveolar crest using RF-echograms. J Clin Periodontol. 1989;16.8:539–44. ISSN:1600-051X.
49. Nguyen K-CT, Shi D, Kaipatur NR, LOU HM, Major PW, Punithakumar K, Le LH. Graph cuts-based segmentation of alveolar bone in ultrasound imaging. In: 2018 IEEE international conference on bioinformatics and biomedicine (BIBM). Piscataway: IEEE; 2018 Dec 3: p. 2049–55. ISBN:1538654881.
50. Nguyen K-CT, Kaipatur NR, Lou EH, Major PW, Punithakumar K, Le LH. Registration of ultrasound and CBCT images for enhancing tooth-periodontinum visualization: a feasibility study. In: 2019 International Conference on Multimedia Analysis and Pattern Recognition (MAPR) 2019 May 9: p. 1–5. IEEE. ISBN:1728118298.
51. Duong DQ, Nguyen K-CT, Kaipatur NR, Lou EH, Noga M, Major PW, Punithakumar K, Le LH. Fully automated segmentation of alveolar bone using deep convolutional neural networks from intraoral ultrasound images. In: 2019 41st Annual International Conference of the IEEE Engineering in Medicine and Biology Society (EMBC) 2019 Jul 23: p. 6632–35. IEEE.
52. Nguyen K-CT, Duong DQ, Almeida FT, Major PW, Pham T-T, Kaipatur NR, Lou EHM, Noga M, Punithakumar K, Le LH. Machine learning-based segmentation of alveolar bone in intraoral ultrasonographs. J Dental Res. May 11, 2020. http://doi.org/10.1177/0022034520920593.
53. Nguyen K-CT, Pacheco-Pűreira C, Kaipatur NR, Cheung J, Major PW, Le LH. Comparison of ultrasound imaging and cone-beam computed tomography for examination of the alveolar bone level: a systematic review. PloS ONE 2018;13.10:e0200596. http://doi.org/10.1371/journal.pone.0200596.